Environmental Science & Technology

pubs.acs.org/est

Article

Sensitivities of Ozone Air Pollution in the Beijing−Tianjin−Hebei Area to Local and Upwind Precursor Emissions Using Adjoint Modeling

Xiaolin Wang, Tzung-May Fu,* Lin Zhang,* Hansen Cao, Qiang Zhang, Hanchen Ma, Lu Shen, Mathew J. Evans, Peter D. Ivatt, Xiao Lu, Youfan Chen, Lijuan Zhang, Xu Feng, Xin Yang, Lei Zhu, and Daven K. Henze

Cite This: https://doi.org/10.1021/acs.est.1c00131

Read Online

ACCESS | Metrics & More | Article Recommendations | Supporting Information

ABSTRACT: Effective mitigation of surface ozone pollution entails detailed knowledge of the contributing precursors' sources. We use the GEOS-Chem adjoint model to analyze the precursors contributing to surface ozone in the Beijing−Tianjin−Hebei area (BTH) of China on days of different ozone pollution severities in June 2019. We find that BTH ozone on heavily polluted days is sensitive to local emissions, as well as to precursors emitted from the provinces south of BTH (Shandong, Henan, and Jiangsu, collectively the SHJ area). Heavy ozone pollution in BTH can be mitigated effectively by reducing NO_x (from industrial processes and transportation), $\geq C_3$ alkenes (from on-road gasoline vehicles and industrial processes), and xylenes (from paint use) emitted from both BTH and SHJ, as well as by reducing CO (from industrial processes, transportation, and power generation) and $\geq C_4$ alkanes (from industrial processes, paint and solvent use, and on-road gasoline vehicles) emissions from SHJ. In addition, reduction of NO_x, xylene, and $\geq C_3$ alkene emissions within BTH would effectively decrease the number of BTH ozone-exceedance days. Our analysis pinpoint the key areas and activities for locally and regionally coordinated emission control efforts to improve surface ozone air quality in BTH.

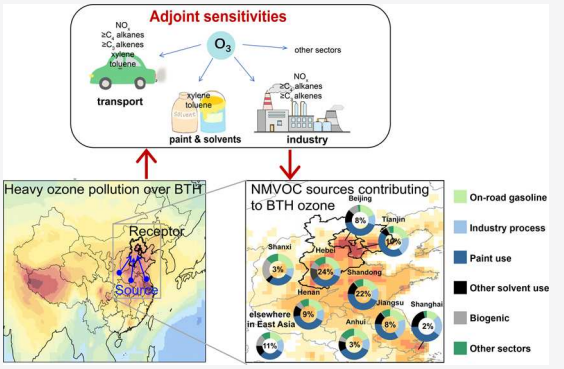

1. INTRODUCTION

The Beijing−Tianjin−Hebei area (BTH) of China has experienced severe summertime surface ozone pollution, which poses serious public health risks.[1−3] Concentrations of air pollutants in BTH exceeded the Chinese national air quality standard for 171 days in 2019, of which surface ozone was the leading pollutant for 83 days.[4] The 90th percentile of the BTH maximum daily 8-hour average (MDA8) ozone concentration in 2019[4] was 196 $\mu g\ m^{-3}$, exceeding the World Health Organization air quality guideline[5] of 100 $\mu g\ m^{-3}$. The Chinese government has recently strengthened BTH ozone pollution prevention, emphasizing the emission reductions of highly active nonmethane volatile organic compounds (NMVOCs).[6] For such efforts to be effective, there must be quantitative understandings of the sources of ozone pollution, including the contributing precursors, their spatial origins, and their emitting activities.

Most analyses of ozone precursors use either observation-based methods (OBMs) or emission-based methods (EBMs).[7] OBM studies use photochemical box models to calculate the maximum incremental reactivity (MIR) or the relative incremental reactivity (RIR) of NMVOCs.[8−12] They then quantify the NMVOCs' contributions to local ozone production based on the locally measured NMVOC concentrations or emission fluxes. Previous OBM studies found $\geq C_3$ alkenes and aromatics to be the largest contributors to ozone formation in the BTH urban area.[8−12] Several studies further employed receptor modeling techniques and found that the observed NMVOCs in the BTH area were mainly emitted from vehicle exhaust, industrial processes, and solvent usage.[8,11,12] However, OBM studies could only characterize the source activities and ozone contributions for the NMVOC mixture observed locally at the receptor site. The spatial origins of these NMVOCs and their transport pathways to the receptor site were not resolved.

By contrast, EBMs simulate the ozone production from precursors using 3-D air quality models. Previous EBM studies

Received: January 6, 2021
Revised: April 12, 2021
Accepted: April 12, 2021

mostly used emission perturbation experiments[13,14] or tagged-tracer experiments[14,15] to quantify the ozone contributions from individual species, sectors, or spatial areas. Studies found that emissions from the industrial and transport sectors contribute significantly to ozone formation over North China.[13,16,17] Recent studies also found that regional transport of ozone or its precursors from central China contributed significantly to BTH surface ozone during summertime persistent ozone pollution events.[14] However, the number of emission-perturbed sensitivity simulations or the number of tagged tracers in EBMs were often limited. As a result, previous EBM studies could not provide detailed species, sector, or spatial information about the precursors contributing to BTH surface ozone.

Meteorology can also modulate the intensity of ozone pollution and the precursors' contributions to ozone at a receptor location.[14,18−20] Gong et al.[14] showed that during persistent ozone pollution events in BTH, the transport of ozone or its precursors from central-eastern China to BTH was enhanced by anomalous southerly winds in North China. Furthermore, they showed that during such events, a 50% reduction of NO_x and NMVOC emissions over central-eastern China could be more effective in reducing BTH surface ozone than a 50% reduction of precursor emissions over North China.[14] Their findings demonstrated the importance of regionally coordinated emission control actions in mitigating BTH ozone pollution. However, their study did not identify the key species or source activities that should be targeted.

Adjoint modeling can provide speciated, sector-resolved, and spatially-resolved information on the precursors contributing to ozone while taking into account the nonlinearity of ozone photochemistry and the meteorological influences on pollutant transport.[21−23] Wang et al.[24] first applied the adjoint of the Community Multiscale Air Quality (CMAQ) model to calculate the sensitivity of monthly mean surface ozone to NO_x and NMVOC emissions in five Chinese receptor areas in June 2010. They concluded that reductions in NO_x and NMVOC emissions would both help mitigate ozone pollution over the BTH, Yangtze River Delta (YRD), and Pearl River Delta (PRD) areas. However, they did not show the spatial and sectorial origins of the major precursors contributing to ozone in each of those receptor areas. In addition, Chinese precursor emissions have changed significantly in recent years,[25,26] such that the sensitivity of ozone should be reevaluated. Adjoint sensitivity analysis has also been used in the source apportionment of Chinese aerosols[27,28] and of health-related air pollutants in other countries.[29,30]

In this study, we use the GEOS-Chem chemical transport model's adjoint to analyze the sensitivity of population-weighted BTH ozone to regional precursor emissions in June 2019 under three different levels of ozone pollution severity: (1) heavily polluted, (2) slightly polluted, and (3) non-exceedance. By separately analyzing the ozone sensitivities on slightly and heavily polluted days, we seek to differentiate the emission control strategies for reducing the number of ozone exceedance days (the criteria by which local air quality management's effectiveness is evaluated) and for mitigating severe ozone pollution. We focus on the year 2019 to better reflect recent Chinese emissions and their impacts on surface ozone. We assess the sensitivity of BTH ozone to various precursors, from different source areas, and from different source activities to pinpoint the emission reduction targets for effective ozone mitigation.

2. METHODS

2.1. Surface Ozone Observations. We analyze hourly surface ozone measurements at 694 sites in 136 cities over North China during June 2019. The measurements were managed by the China National Environmental Monitoring Center (http://106.37.208.233:20035/). We remove hourly concentration outliers at each site that exceeded the 2019 annual mean ozone concentrations by more than four standard deviations, following one of the three quality control protocols in Lu et al.'s study.[31] The other two protocols are not applied because one does not remove any measurements, and the other removes measurements that appear to be valid. We average sites to calculate the city−mean hourly ozone concentrations and sample the model results at city centers.

We define the daily exceeded multiples of MDA8 ozone (EM_{MDA8_O3}) in each city as[32]

$$EM_{MDA8\_O3} = \frac{C - S}{S} \times 100\% \quad (1)$$

where C is the daily MDA8 ozone concentrations in that city in units of parts per billion. S is the national ambient air quality standard of MDA8 ozone concentration for urban locations, which is 160 μg m^{-3} at 298 K and 1013 hPa[33,34] and is equivalent to 81.6 ppb. We define days when $EM_{MDA8\_O3} \leq 0$ as non-exceedance days, days when $0 < EM_{MDA8\_O3} \leq 10\%$ (i.e., MDA8 ozone between 81.6 and 89.7 ppb) as slightly polluted, and days when $EM_{MDA8\_O3} \geq 20\%$ (i.e., MDA8 ozone exceeding 97.9 ppb) as heavily polluted.

2.2. Tropospheric Column NO_2 and Formaldehyde Data from TROPOMI. We analyze the daily tropospheric formaldehyde and NO_2 column concentrations[35,36] observed by the TROPOspheric Monitoring Instrument (TROPOMI) over China on days of different ozone pollution severity to examine the difference in precursor abundance and NO_x-sensitivity of surface ozone production.[37−39] TROPOMI is a nadir-viewing spectrometer aboard the polar-orbiting Sentinel-5 Precursor satellite (equator crossing at 13:30 local time).[40] The level 2 NO_2 and formaldehyde offline data used here has near-daily global coverage and nadir pixel resolution of 7 km × 3.5 km.[40] We remove pixels with a quality assurance value (qa_value)[41] less than 0.5 and calculate the daily tropospheric NO_2 and formaldehyde column concentrations at 0.25° resolution.

2.3. The GEOS-Chem Forward Model and Its Adjoint. We use the nested-grid capability (0.3125° longitude × 0.25° latitude, 47 vertical levels) of the GEOS-Chem chemical transport model[42] and its adjoint[27,43] to simulate BTH surface ozone and its sensitivity in June 2019 (the model domain is shown in Figure S1). The GEOS-Chem forward model and its adjoint (v35n) used here were initially developed as v8.2.1 of GEOS-Chem,[43,44] which included a detailed tropospheric ozone-NO_x-NMVOC-aerosol chemical mechanism.[42,45] The NMVOC precursors in GEOS-Chem v8.2.1 include ethane, propane, $\geq C_4$ alkanes, $\geq C_3$ alkenes, isoprene, acetone, $\geq C_2$ aldehyde, formaldehyde, and methyl ethyl ketone. We add here the gas-phase chemistry of benzene, toluene, and xylene from the Regional Atmospheric Chemistry Mechanism, version 2 (RACM2).[46] Text S1 further describes the setups and updates to the GEOS-Chem model used in our study.

Chinese monthly anthropogenic emissions of NO_x, NMVOC, CO, and other pollutants are from the Multi-resolution Emission Inventory for China (MEIC)[25,47] for the

https://doi.org/10.1021/acs.est.1c00131
Environ. Sci. Technol. XXXX, XXX, XXX−XXX

Table 1. Description of Adjoint Sensitivity Simulations

simulations	ozone pollution levels	cost functions	MDA8 O_3 concentrations (ppb)
BTH_N	non-exceedance in BTH	population-weighted BTH MDA8 O_3 on EM ≤ 0 days	67.2 (population-weighted)
BTH_S	slight pollution in BTH	population-weighted BTH MDA8 O_3 on 0 < EM ≤ 10% days	82.5 (population-weighted)
BTH_H	heavy pollution in BTH	population-weighted BTH MDA8 O_3 on EM ≥ 20% days	106.4 (population-weighted)
B_H	heavy pollution in Beijing	Beijing MDA8 O_3 on EM ≥ 20% days	110.4
T_H	heavy pollution in Tianjin	Tianjin MDA8 O_3 on EM ≥ 20% days	110.1
S_H	heavy pollution in Shijiazhuang	Shijiazhuang MDA8 O_3 on EM ≥ 20% days	110.5

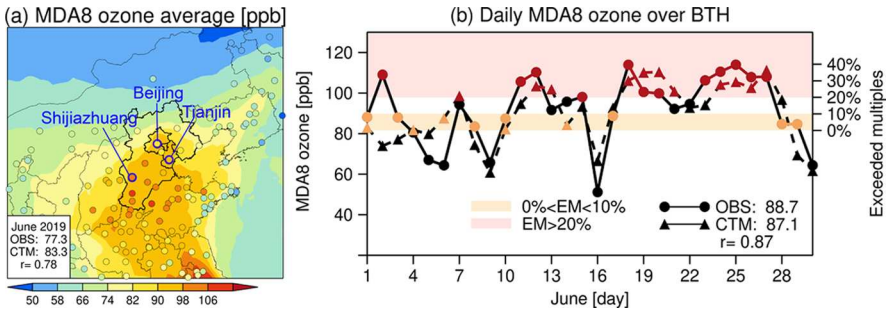

Figure 1. (a) Observed (symbols) and simulated (filled contours) MDA8 surface ozone concentrations over North China in June 2019. Mean observed and simulated MDA8 ozone concentrations at the surface sites, and their spatial correlations, are shown inset. The bold black line denoted the BTH area. Symbols circled in blue demarcate the city centers of Beijing, Tianjin, and Shijiazhuang. (b) Time series of the observed (circles) and simulated (triangles) BTH surface MDA8 ozone concentrations in June 2019. The orange and red areas indicate ranges of ozone concentrations when $0 < EM_{MDA8\_O3} \leq 10\%$ (slightly polluted) and $EM_{MDA8\_O3} \geq 20\%$ (heavily polluted), respectively. The orange and red symbols indicate the days when the observed (circles) or the simulated (triangles) ozone concentrations fall into these two pollution levels, respectively.

year 2017 (Figure S2). MEIC is based on provincial-level activity statistics and includes emissions from power generation, industries, transport, and residential activities with 0.25° horizontal resolution. NMVOC speciation in MEIC is based on Chinese emission profiles.[47] Previous evaluations showed that MEIC is able to represent the magnitudes and seasonal/interannual variation of Chinese emissions.[48,49] Anthropogenic emissions outside China are from MIX-Asian inventory for 2010.[50] Natural precursor emissions from vegetation, soil, and lightning are calculated online in GEOS-Chem (Figure S2).[51−53] Emissions from open biomass burning are from the Global Fire Emissions Dataset version 4.1 (GFED4s) for the year 2019 at 0.25° spatial resolution.[54]

2.4. Adjoint Sensitivity Simulations. We use the GEOS-Chem adjoint model[27,43] to calculate the sensitivity of ozone to precursor emissions. A brief description of the adjoint methodology is given in Text S2. Consider a cost function, J, as the average surface ozone concentration over the targeted receptor area during a targeted period:

$$J = \overline{C_{t,O_3}},\ t \in \Omega_t \tag{2}$$

where C_{t,O_3} is the surface ozone concentration over the targeted area at time t, while Ω_t is the time domain during which the cost function is evaluated. In this study, the adjoint sensitivities of ozone represent the derivatives of the surface ozone concentration at the targeted receptor area (i.e., cost function in eq 2) to emissions, $\frac{\partial J}{\partial \boldsymbol{E}_i}$, where $\boldsymbol{E}_i$ is the emission of species i at each grid from each sector. To reflect the influence of a small change in emissions to the actual ozone concentrations, we multiply the adjoint sensitivities by 10% of $\boldsymbol{E}_i$. In the analysis below, we focus on this quantity, $\frac{\partial J}{\partial \boldsymbol{E}_i} \times \boldsymbol{E}_i \times 10\%$, which reflects the ozone change over the receptor area due to a 10% increase in emissions of species i at each source grid. In Section 3.4, we further attribute the sensitivity of ozone to sectorial and subsectorial emissions by apportioning $\frac{\partial J}{\partial \boldsymbol{E}_i} \times \boldsymbol{E}_i \times 10\%$ to the relative contribution of each sector/subsector to $\boldsymbol{E}_i$ at each emitting grid.

We conduct a forward simulation and 6 adjoint experiments for June 2019 (Table 1). The forward simulation is spun up between March and May 2019. We integrate the adjoint sensitivities backwards in time from June 30 to May 16, 2019 to account for the impacts on June surface ozone from precursors emitted in June and late May. In experiments BTH_N, BTH_S, and BTH_H, we define the cost function (J) as the population-weighted surface MDA8 ozone concentration over the BTH area during days when the simulated BTH EM_{MDA8_O3} were ≤0, between 0 and 10%, and ⩾20%, respectively. Analyzing the sensitivity of population-weighted ozone highlights the impacts on human exposure. Gridded population data (Figure S3) for the year 2015 are from the Center for International Earth Science Information Network of Columbia University (https://doi.org/10.7927/H4JW8BX5). In experiments B_H, T_H, and S_H (Text S3 and Figure S4), we examine the ozone sensitivities during the heavily polluted days in three major BTH cities: Beijing, Tianjin, and Shijiazhuang (the capital of Hebei province and densely populated), respectively (Figure 1a).

3. RESULTS

3.1. Validation of Simulated Ozone Concentrations over North China. Figure 1 shows the monthly mean surface MDA8 ozone concentrations simulated by the GEOS-Chem forward model for June 2019 and compare them against the surface observations. The observed June surface MDA8 ozone concentrations exceed 82 ppb over BTH and the surrounding Shandong and Henan. In southern Hebei and western

https://doi.org/10.1021/acs.est.1c00131
Environ. Sci. Technol. XXXX, XXX, XXX−XXX

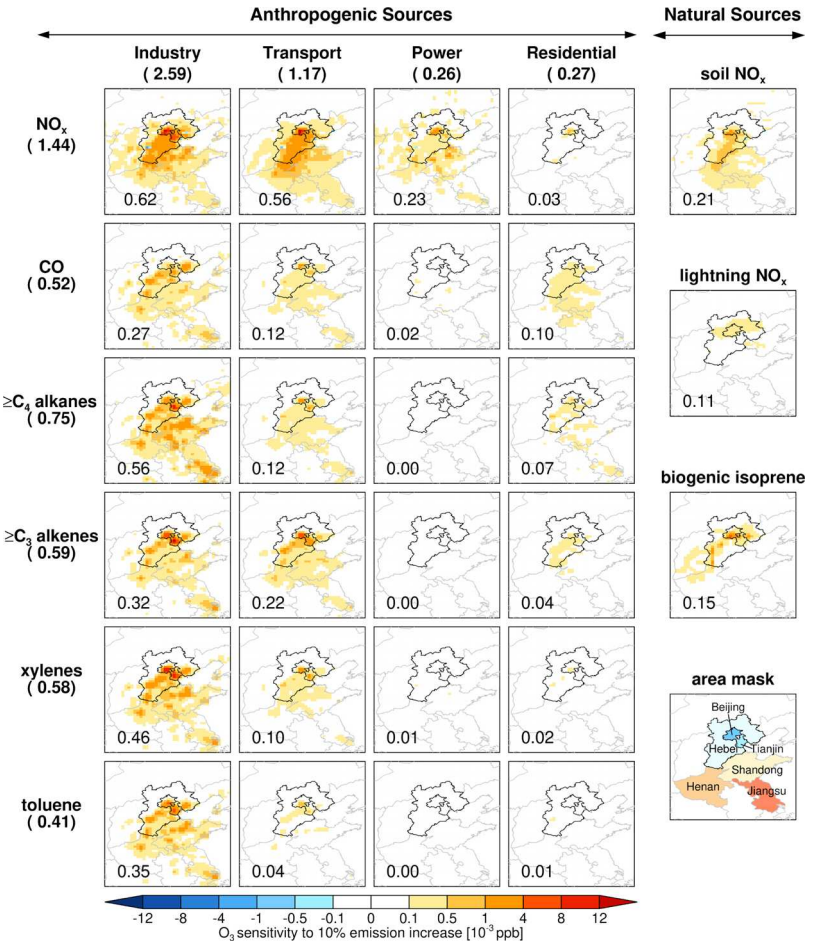

Figure 2. Sensitivities of population-weighted BTH MDA8 surface ozone concentrations to the 10% increase of precursor emissions (unit, 10^{-3} ppb) over North China on BTH heavily polluted days in June 2019. Sensitivities are separated by sectors and chemical species at the model resolution (0.3125° longitude × 0.25° latitude). The numbers in parentheses represent the sum of sensitivities (unit, ppb) for the species or from the sector over the model domain. Black lines demarcate the BTH area. The bottom-right panel shows the provinces/cities in North China.

Shandong, the observed peak ozone concentrations exceed 98 ppb. The model generally reproduced the observed spatial distribution of ozone over North China (Figure 1a, spatial correlation is r = 0.78 for the 136 cities). Over the 13 cities in the BTH area, the simulated monthly mean MDA8 ozone concentration is 87.1 ppb, which is in good agreement with the observed value of 88.7 ppb. The model overestimates the observed ozone concentrations in the area south of BTH. The reason for this overestimation is yet unclear but may reflect some misrepresentation of local emissions or chemistry;[55] we address the associated uncertainties in the Discussion.

Figure 1b shows the time series of the observed and simulated MDA8 ozone and the daily EM_{MDA8_O3} values in BTH in June 2019. The GEOS-Chem forward model captures the day-to-day variation of ozone concentrations (temporal correlation against daily observations, r = 0.87), including, most critically, the periods during which slight and heavy ozone pollution occurred. Observations show heavy ozone pollution on the 2nd, 11th, 12th, 15th, 18th−20th, and 23rd−27th of June (12 days) and slight ozone pollution on the 1st, 3rd, 8th, 10th, 17th, 28th, and 29th of June (7 days). The model simulates heavy ozone pollution on the 7th, 12th, 13th, 18th−21st, and 24th−27th of June (11 days) and slight ozone pollution on the 1st, 4th, 6th, 10th, and 14th of June (5 days). The above validation of the simulated ozone concentrations supports our use of the GEOS-Chem adjoint for BTH ozone source apportionment.

We select the dates when the simulated BTH MDA8 ozone is non-exceeding, slightly polluted, and heavily polluted as the dates (the temporal domains Ω_t in eq 2) to calculate the cost functions in the adjoint simulations (Table 1). In the BTH_H, BTH_S, and BTH_N experiments, the simulated values of the cost function are 106.4, 82.5, and 67.2 ppb, respectively. For the B_H, T_H, and S_H experiments, the cost functions are the simulated mean MDA8 ozone concentrations in the corresponding city on heavily polluted days (Figure S4), which are 110.4, 110.1, and 110.5 ppb, respectively.

3.2. Sensitivities of BTH Ozone for Different Levels of Ozone Pollution Severity in June 2019. Figure 2 shows the adjoint sensitivities of population-weighted BTH MDA8 ozone on the heavily polluted days in June 2019. The sensitivities are calculated for individual precursors from each of its source sectors and each grid. For brevity, Figure 2 shows only the 5 NMVOCs to which BTH ozone is most sensitive. The magnitudes of the ozone sensitivities represent the changes in BTH population-weighted MDA8 ozone in response to a 10% increase of emissions at each model grid ($\frac{\partial J}{\partial \boldsymbol{E}_i} \times \boldsymbol{E}_i \times 10\%$). During heavily polluted days, NO_x, CO, and NMVOC precursors emitted from BTH and provinces south of BTH (Shandong, Henan, and Jiangsu, hereafter

https://doi.org/10.1021/acs.est.1c00131
Environ. Sci. Technol. XXXX, XXX, XXX−XXX

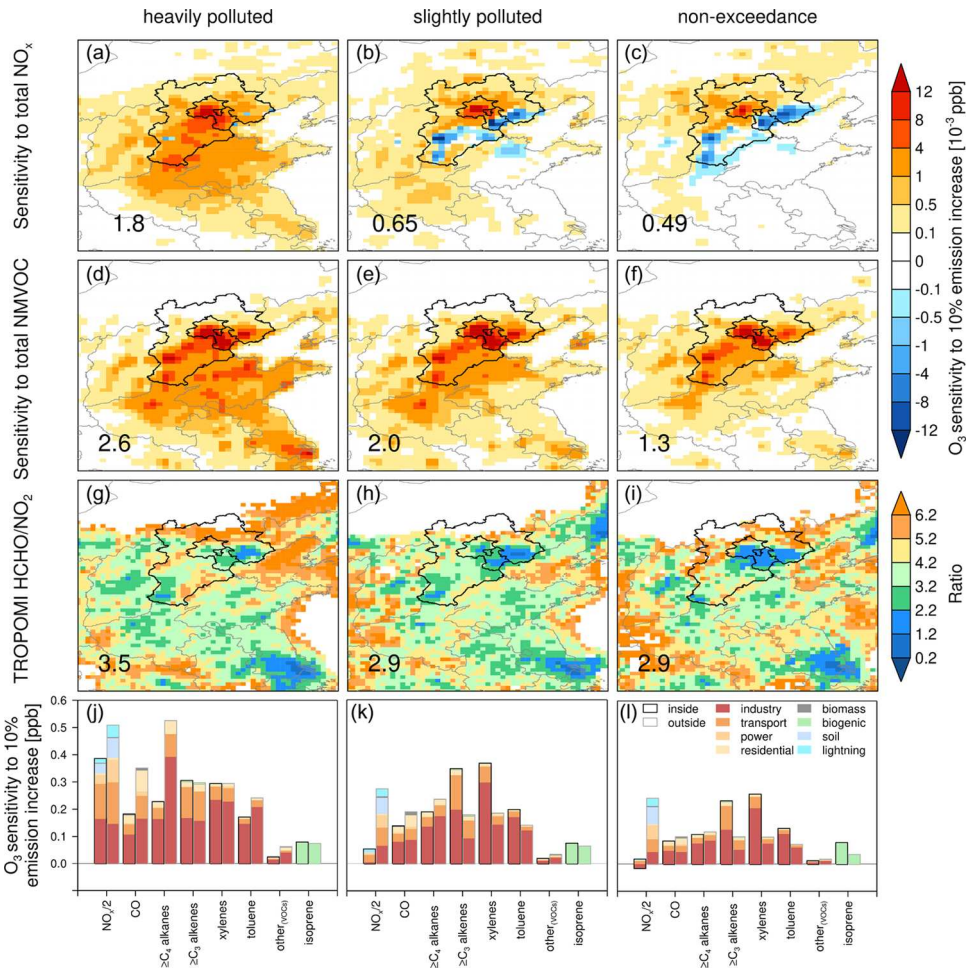

Figure 3. Comparison of adjoint-simulated and satellite-observed sensitivity of BTH ozone for three ozone pollution severity levels in June 2019. The BTH ozone adjoint sensitivities (unit, 10^{-3} ppb) are shown for total NO_x emissions (top row) and total NMVOC emissions (second row); the sums of sensitivities over the simulation domain (unit, ppb) are shown inset. The bar charts (bottom row) summarize sensitivities to precursors from various sectors emitted inside (black boxes) and outside (grey boxes) the BTH area. Third row: TROPOMI-observed ratios of tropospheric HCHO to NO_2 column concentrations (only grids with tropospheric NO_2 column >1.5 × 10^{15} molec cm^{-2} are shown); the population-weighted $HCHO/NO_2$ ratios over the BTH are shown inset.

referred to as the SHJ area) all contribute positively to BTH ozone. The ozone sensitivities to 10% anthropogenic emission increases of NMVOCs, NO_x, and CO over East Asia (domain shown in Figure S1) are 2.40, 1.44, and 0.52 ppb, respectively. During heavily polluted days, the largest NMVOC contributor to BTH ozone is ≥C_4 alkanes (0.75 ppb), followed by ≥C_3 alkenes (0.59 ppb), xylenes (0.58 ppb), and toluene (0.41 ppb). Furthermore, most of the ozone sensitivity are associated with precursors emitted from industrial activities (2.59 ppb) and transportation (1.17 ppb). The sensitivities of ozone to natural and biomass burning (not shown in Figure 2) emissions are much smaller, except for the sensitivities to biogenic isoprene (0.15 ppb) and soil-NO_x (0.21 ppb). This finding is consistent with a previous model study,[56] which found anthropogenic precursors' contributions to BTH ozone to be much larger than those of natural precursors during heavy ozone pollution days.

In contrast, on slightly polluted and non-exceedance days, BTH ozone is mostly sensitive to precursors emitted within BTH, with relatively smaller contributions from precursors emitted from the adjacent Henan and northern Shandong (Figures S5 and S6). The ozone sensitivities to emissions from Jiangsu and other parts of Shandong are much smaller than those on heavily polluted days. On slightly polluted and non-exceedance days, the most important anthropogenic NMVOC contributors to BTH ozone sensitivity are xylenes (0.55 and 0.35 ppb, respectively) and ≥C_3 alkenes (0.52 and 0.33 ppb, respectively) (Figures S5 and S6). Ozone and precursors transported to BTH from outside North China have small but non-negligible contributions to BTH ozone under all levels of ozone pollution severity (Text S4).

On less polluted days, we find that BTH ozone is more VOC-limited (i.e., NO_x-saturated) than it is on heavily polluted days (Figure 3): the ozone sensitivities to the 10% increase in anthropogenic NMVOC emissions (2.0 and 1.3 ppb, respectively) are three times the sensitivities to NO_x (0.65 and 0.49 ppb, respectively) on less polluted days. Furthermore, on less polluted days, BTH ozone is positively sensitive to NO_x emitted from northern BTH but negatively sensitive to NO_x emitted from southern BTH (Figure 3b,c). Previous studies have demonstrated satellite-observed $HCHO/NO_2$ ratios as useful indicators for the ozone formation regime.[37−39] Wang et al.[57] recommended $HCHO/NO_2$ < 2.3 as an indication for VOC-limited ozone formation, $HCHO/NO_2$ > 4.2 for NO_x-limited ozone formation, and $HCHO/NO_2$ between 2.3 and 4.2 as an indication for transitional ozone formation. We find

https://doi.org/10.1021/acs.est.1c00131
Environ. Sci. Technol. XXXX, XXX, XXX−XXX

the $HCHO/NO_2$ ratios observed by TROPOMI over the BTH area to be 3.5 on heavily polluted days and 2.9 on less polluted days in June 2019 (Figure 3g–i), confirming the larger sensitivity of BTH ozone to NO_x during heavy pollution. In Beijing, ozone formation changed from a VOC-limited regime ($HCHO/NO_2 < 2.3$) on non-exceeded days to a transitional regime ($HCHO/NO_2$ between 2.3 and 4.2) on heavily polluted days.

3.3. Impacts of Meteorology on BTH Ozone Sensitivity. Our analyses above show that the transport of pollutants from the SHJ area aggravates BTH ozone during heavily polluted days, demonstrating the importance of regional transport to BTH ozone air quality. On non-exceedance days, the prevailing wind over the BTH area is northwesterly, which transports relatively low ozone air to the BTH area (Figure S7a). When the BTH area is heavily polluted, the local wind changes to southerly. We find that this anomalous southerly wind over the BTH area during heavily polluted days is associated with a surface high-pressure anomaly over Shandong and the East China Sea (Figure S7d). This surface anticyclone is also associated with a positive geopotential anomaly at 500 hPa and a >5 °C surface temperature anomaly over Northeastern China (Figure S7e,f). We further find that the meteorological anomalies associated with slightly polluted days are similar to those associated with heavily polluted days, except that they are of smaller amplitudes. Therefore, these anomalous meteorological patterns may be used as indicators to forecast ozone exceedance events. Previous studies also found that anomalous southerly winds could transport ozone or its precursors from central-eastern China (mostly corresponding to the SHJ area) to the BTH area during summertime persistent ozone pollution events.[14,18]

Our adjoint analyses show that the enhanced pollutant advection from the SHJ to the BTH area and the meteorological conditions favoring local photochemical production and biogenic emissions all contribute to the high ozone pollution over the BTH area. On heavily polluted days in BTH, NO_x, CO, and NMVOC precursors emitted from SHJ contributed 31, 39, and 39%, respectively, of the total BTH ozone sensitivities. A large fraction of this enhanced SHJ contribution is associated with the advection of CO and longer-lived NMVOC precursors from SHJ (Figures 2 and 3j and Figure S8). Also, on heavily polluted days, the overhead anticyclone suppresses the ventilation of the BTH boundary layer. This suppressed ventilation leads to accumulated surface NMVOC concentrations (Figure S9), which increases the sensitivity of BTH ozone to NO_x. TROPOMI observations also indicate this strengthening of BTH ozone photochemistry due to the accumulation of NMVOCs in BTH on heavily polluted days. The tropospheric HCHO column concentrations over BTH are much higher on heavily polluted days than on less polluted days, while tropospheric NO_2 columns show less difference (Figure S10). Enhanced biogenic isoprene emissions at warmer temperatures may also play a role. Figure S9 shows that the BTH surface isoprene concentration is much higher on heavily polluted days than on less polluted and non-exceedance days. Although the ozone sensitivity to biogenic isoprene changes a little under the different pollutant levels (total of 0.11 to 0.15 ppb in Figure 3j–l), the larger isoprene emissions under warmer temperatures still enhance BTH ozone on heavily polluted days. However, overall, the BTH ozone sensitivity to isoprene is smaller than that to CO and anthropogenic NMVOCs (Figures 2 and 3j).

3.4. Strategic Emission Reduction to Mitigate BTH Ozone Pollution: Provincial/Municipal Targets and Sector/Subsector Targets. Our adjoint methodology quantifies the contributions to BTH ozone from individual precursors with their spatial and sectorial origins resolved. This information provides targeted, actionable guidance for effective mitigation of BTH ozone. Figure 3j summarizes the BTH ozone sensitivities to individual precursors by their source sectors and spatial origins (either inside or outside the BTH area) on heavily polluted days. The ozone sensitivities to precursors emitted outside the BTH area mainly involve those emitted in the SHJ area; contributions from other Chinese provinces are relatively small (Figure S8a). On heavily polluted days, BTH ozone is highly sensitive to NO_x emissions from industrial activities and transportation in both BTH and SHJ. The BTH ozone sensitivities to CO and $\geq C_4$ alkanes emitted from the SHJ area are twice as large as the ozone sensitivities to these precursors emitted from the BTH area (Figure 3j). Both CO and $\geq C_4$ alkanes are primarily emitted by industrial activities. They are effectively transported from the SHJ area to affect the BTH area due to their relatively long chemical lifetimes. For the highly reactive NMVOCs ($\geq C_3$ alkenes, xylenes, and toluene), the contributions to BTH ozone sensitivity from inside and outside the BTH are comparable. These highly reactive NMVOCs are mostly emitted by industrial activities and transportation. Our results suggest that to mitigate heavy BTH ozone pollution, the most effective measures entail reducing NO_x and reactive NMVOC ($\geq C_3$ alkenes, xylenes, and toluene) emissions in both the BTH and the SHJ areas, as well as CO and $\geq C_4$ alkanes emitted from the SHJ area. A 10% reduction of these precursor emissions would decrease the simulated BTH ozone on heavily polluted days by 4.9 ppb and decrease the number of heavy pollution days from 11 days to 7 days in June 2019, according to our adjoint analyses. Thus, the adjoint sensitivities point to a way to mitigate heavy BTH ozone pollution, which may be adopted as short-term goals or emergency response measures under government-led regional coordination.

Figure 3k,l shows the BTH ozone sensitivity to regional precursors on slightly polluted and non-exceedance days, with the precursors' provincial/municipal origins shown in Figure S8. Again, we find that on these less polluted days, the BTH MDA8 ozone production is more VOC-limited and less sensitive to emissions from outside the BTH area. BTH ozone on less polluted days is generally positively sensitive to NO_x but shows negative sensitivities to the large industrial NO_x emissions over the southern BTH area (Figure S11). The highly reactive NMVOCs (xylenes, $\geq C_3$ alkenes, and toluene) emitted by industrial activities and transportation inside the BTH area are the largest contributors to BTH ozone sensitivity. The sensitivities to CO and $\geq C_4$ alkanes emitted inside and outside the BTH area are roughly equivalent. Compared to the sensitivities on heavily polluted days, the overall sensitivities of BTH ozone to CO and $\geq C_4$ alkanes are greatly diminished. Such difference in the ozone sensitivities reflects the less advection of longer-lived precursors from the SHJ area to affect the BTH area on the less polluted days. Our analyses show that to lower the BTH surface ozone concentrations on slightly polluted days (thus decreasing the number of ozone-exceeding days), BTH emissions of NO_x and highly reactive anthropogenic NMVOCs should be reduced.

https://doi.org/10.1021/acs.est.1c00131
Environ. Sci. Technol. XXXX, XXX, XXX−XXX

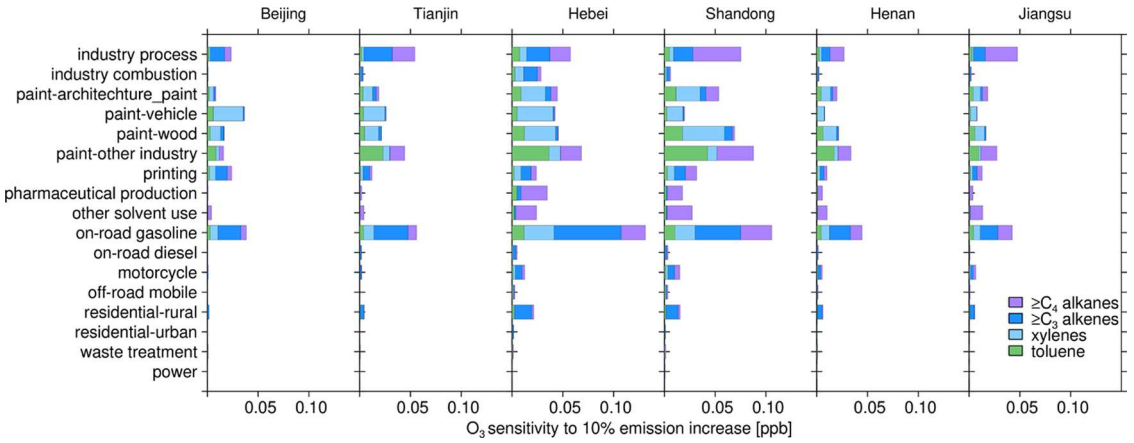

Figure 4. Sensitivities of BTH ozone to four anthropogenic NMVOC species ($\geq C_4$ alkanes, $\geq C_3$ alkenes, xylenes, and toluene) on heavily polluted days. Sensitivities are segregated for the emitting activities and the provinces/cities of emission.

Such effort will help the local agencies achieve their air quality attainment goals in the short term and provide an actionable pathway for the local government to improve the annual mean ozone air quality. Strong control of BTH reactive NMVOC emissions is also needed to offset the side effects of reduced NO_x over southern BTH during less polluted days. Our adjoint analyses show that the sensitivities of BTH ozone to the 10% anthropogenic NO_x emission increase over southern BTH are −0.19 and −0.18 ppb on slightly polluted and non-exceedance days, respectively (Figure 3b); the sensitivities of BTH ozone to the 10% anthropogenic NMVOC emission increase over southern BTH is 0.60 and 0.50 ppb on slightly polluted and non-exceedance days, respectively. Thus, to offset every 10% of NO_x reduction over southern BTH, an additional $1/3 \times 10\%$ reduction of NMVOC emissions is required on less polluted days.

Our analyses above identify the key NMVOC species whose emission must be reduced. However, NMVOC species are emitted from a wide range of anthropogenic activities. As such, species-based emission reductions may be difficult to implement and manage. In comparison, sector/subsector-based emission reduction actions target key emitting activities, where emissions can be controlled by improving/substituting processes and technologies. To further pinpoint which sectors/subsectors should be controlled with high priority, we map the spatially resolved ozone-to-NMVOC sensitivity to 17 subsectors, including 9 industrial subsectors, 4 transport subsectors, 3 residential subsectors, and the power generation sector. The results are shown in Figure 4 for the 4 NMVOC species most important to BTH ozone on heavily polluted days ($\geq C_4$ alkanes, $\geq C_3$ alkenes, xylenes, and toluene). For all cities and provinces in North China, the activities with the largest contributions to BTH ozone sensitivity are paint use (for architecture, vehicles, wood products, and other products), on-road gasoline vehicles, and industrial processes (here mainly including coking, oil refinement, distribution and storage of oil/gas, and chemical production). Reducing emissions associated with paint use will decrease ozone sensitivities to xylenes and toluene most effectively. Reducing emissions from on-road gasoline vehicles and industrial processes will decrease the ozone sensitivity to $\geq C_3$ alkene emissions. Finally, $\geq C_4$ alkanes from the SHJ area contributed to BTH ozone during heavily polluted days; their emissions should be reduced by targeting industrial processes, paint and solvent use, and pharmaceutical production. Some of these NMVOCs are themselves toxic; reducing their emissions will also mitigate the local communities' health risks associated with exposure to those toxic NMVOCs.[58]

Our adjoint sensitivity analyses can also be applied to individual cities to better guide the city's air quality management efforts. Figures S12−S14 show the ozone sensitivities for Beijing, Tianjin, and Shijiazhuang, on their respective heavily polluted days. Figure S15 summarizes the ozone sensitivities in each city to emissions from local and surrounding provinces and cities. On heavily polluted days, the MDA8 surface ozone concentrations in a particular city are most sensitive to emissions from within that city. For Beijing, ozone is most sensitive to local emissions of NO_x, xylenes, and $\geq C_3$ alkenes; reducing both NO_x and NMVOC emissions in Beijing will help mitigate severe local ozone pollution. OBM studies of ozone sensitivity before the year 2013 mostly found ozone production in Beijing to be NO_x-saturated.[59,60] However, since the year 2013, there have been strong measures to reduce industrial and vehicular NO_x emissions in Beijing. The observed surface NO_2 concentration in Beijing decreased at an annual rate of -1.7 ppb year^{-1} during 2013 to 2019.[61] More recent observations indicate that Beijing's ozone production may have migrated to the transition regime or the NO_x-limited regime, especially in summer when the photochemical production of ozone is most active.[39,59,61] Our finding that Beijing's surface ozone is positively sensitive to local NO_x emissions on heavily polluted days is consistent with these recent observational studies. In contrast, the heavy ozone pollutions in Tianjin and Shijiazhuang are more VOC-limited, such that reducing local NMVOC emissions would be more effective in mitigating the ozone pollution within these two cities. Our results highlight the importance of reducing reactive NMVOC emissions in conjunction with reducing NO_x emissions to improve the ozone air quality in the cities in BTH.

4. DISCUSSION

We use the adjoint of the GEOS-Chem chemical transport model to quantify BTH ozone sensitivities to regional precursors, resolving the chemical identities, spatial origins, and activity origins of those precursors. We find that the ozone sensitivities on days with different ozone pollution severities differ by the contributing precursors' identities and spatial

https://doi.org/10.1021/acs.est.1c00131
Environ. Sci. Technol. XXXX, XXX, XXX−XXX

origins. Our results highlight the dependence of the ozone-precursor relationship on regional meteorology. We also identify the key emitting activities contributing to BTH ozone pollution; these activities should be the priority targets for process substitution or application of emission reduction technologies. However, we emphasize that the accuracy of the adjoint sensitivity analyses depends on the accuracy of the emission inventories. In this study, our model simulations show high tropospheric NO_x concentration and NO_x-saturated ozone production over the YRD area (Figure S16), consistent with TROPOMI observations (Figures 3g–i and S10). However, our simulated tropospheric HCHO column concentrations are higher over the YRD area than over the BTH area (Figure S16), while TROPOMI observes higher HCHO concentrations over the BTH area (Figure S10). This inconsistency suggests that the NMVOC emissions over the YRD area may be overestimated, which may partially account for the ozone overestimation in the south of BTH (Figure 1a) and may lead to positive biases of BTH ozone sensitivity to YRD NMVOC precursors. Further evaluation of NMVOC emissions over the south of BTH is needed. As Chinese emissions of precursors continue to change as driven by evolving technology and emission reduction policies,[25,62] especially as driven by the Chinese initiative toward carbon neutrality, it is crucial that emission inventories and our adjoint analysis be timely updated to reflect the impact on ozone pollution.

Our methodology can be applied to other areas in China suffering from heavy ozone pollution. Also, several studies showed that the sensitivity of ozone production varies significantly with altitude. Over some polluted areas, ozone formation may be NO_x-limited in the upper boundary layer, while being VOC-limited in the lower boundary layer.[63] As a result, tropospheric ozone and the atmospheric oxidation capacity may not respond to precursor emission controls in the same way as surface ozone does. The adjoint methodology could provide a more comprehensive understanding of the sensitivities of ozone and regional oxidation capacity to emissions and meteorology.

■ ASSOCIATED CONTENT

Supporting Information

The Supporting Information is available free of charge at https://pubs.acs.org/doi/10.1021/acs.est.1c00131.

Updates to the GEOS-Chem model updates and setup of simulations, description of the adjoint model methodology and adjoint experiments, impacts on BTH surface ozone from outside North China, simulated surface ozone concentration with aromatics, monthly precursor emissions, population density, sensitivities of BTH ozone on slightly polluted and non-exceedance days, averaged and anomalous meteorological patterns, sensitivities of BTH ozone from provinces/cities, average diurnal cycles of simulated tracer concentrations in the BTH, TROPOMI tropospheric HCHO and NO_2 column concentrations, monthly anthropogenic emissions of NO_x and major NMVOCs, sensitivity of municipal MDA8 surface ozone to 10% precursor emissions increases, and simulated tropospheric HCHO and NO_2 column concentrations and HCHO to NO_2 ratio (PDF)

■ AUTHOR INFORMATION

Corresponding Authors

Tzung-May Fu − *State Environmental Protection Key Laboratory of Integrated Surface Water-Groundwater Pollution Control, School of Environmental Science and Engineering, Southern University of Science and Technology, Shenzhen, Guangdong 518055, China; Guangdong Provincial Key Laboratory of Soil and Groundwater Pollution Control, School of Environmental Science and Engineering, Southern University of Science and Technology, Shenzhen, Guangdong 518055, China;* orcid.org/0000-0002-8556-7326; Email: fuzm@sustech.edu.cn

Lin Zhang − *Department of Atmospheric and Oceanic Sciences, School of Physics, Peking University, Beijing 100871, China;* orcid.org/0000-0003-2383-8431; Email: zhanglg@pku.edu.cn

Authors

Xiaolin Wang − *Department of Atmospheric and Oceanic Sciences, School of Physics, Peking University, Beijing 100871, China;* orcid.org/0000-0001-6772-0350

Hansen Cao − *Department of Mechanical Engineering, University of Colorado Boulder, Boulder, Colorado 80309, United States*

Qiang Zhang − *Ministry of Education Key Laboratory for Earth System Modeling, Center for Earth System Science, Tsinghua University, Beijing 100084, China*

Hanchen Ma − *Ministry of Education Key Laboratory for Earth System Modeling, Center for Earth System Science, Tsinghua University, Beijing 100084, China*

Lu Shen − *Harvard John A. Paulson School of Engineering and Applied Sciences, Harvard University, Cambridge, Massachusetts 02138, United States*

Mathew J. Evans − *Wolfson Atmospheric Chemistry Laboratories, Department of Chemistry, University of York, York YO10 5DD, U.K.; National Centre for Atmospheric Science, Department of Chemistry, University of York, York YO10 5DD, U.K.;* orcid.org/0000-0003-4775-032X

Peter D. Ivatt − *Wolfson Atmospheric Chemistry Laboratories, Department of Chemistry, University of York, York YO10 5DD, U.K.; National Centre for Atmospheric Science, Department of Chemistry, University of York, York YO10 5DD, U.K.*

Xiao Lu − *Harvard John A. Paulson School of Engineering and Applied Sciences, Harvard University, Cambridge, Massachusetts 02138, United States;* orcid.org/0000-0002-5989-0912

Youfan Chen − *Sichuan Academy of Environmental policy and planning, Chengdu, Sichuan 610041, China*

Lijuan Zhang − *Shanghai Central Meteorological Observatory, Shanghai 200030, China; State Environmental Protection Key Laboratory of Integrated Surface Water-Groundwater Pollution Control, School of Environmental Science and Engineering, Southern University of Science and Technology, Shenzhen, Guangdong 518055, China; Guangdong Provincial Key Laboratory of Soil and Groundwater Pollution Control, School of Environmental Science and Engineering, Southern University of Science and Technology, Shenzhen, Guangdong 518055, China*

Xu Feng − *Department of Atmospheric and Oceanic Sciences, School of Physics, Peking University, Beijing 100871, China; State Environmental Protection Key Laboratory of Integrated Surface Water-Groundwater Pollution Control, School of*

https://doi.org/10.1021/acs.est.1c00131
Environ. Sci. Technol. XXXX, XXX, XXX−XXX

Environmental Science and Engineering, Southern University of Science and Technology, Shenzhen, Guangdong 518055, China; Guangdong Provincial Key Laboratory of Soil and Groundwater Pollution Control, School of Environmental Science and Engineering, Southern University of Science and Technology, Shenzhen, Guangdong 518055, China

Xin Yang − *State Environmental Protection Key Laboratory of Integrated Surface Water-Groundwater Pollution Control, School of Environmental Science and Engineering, Southern University of Science and Technology, Shenzhen, Guangdong 518055, China; Guangdong Provincial Key Laboratory of Soil and Groundwater Pollution Control, School of Environmental Science and Engineering, Southern University of Science and Technology, Shenzhen, Guangdong 518055, China;* orcid.org/0000-0002-9173-1188

Lei Zhu − *State Environmental Protection Key Laboratory of Integrated Surface Water-Groundwater Pollution Control, School of Environmental Science and Engineering, Southern University of Science and Technology, Shenzhen, Guangdong 518055, China; Guangdong Provincial Key Laboratory of Soil and Groundwater Pollution Control, School of Environmental Science and Engineering, Southern University of Science and Technology, Shenzhen, Guangdong 518055, China*

Daven K. Henze − *Department of Mechanical Engineering, University of Colorado Boulder, Boulder, Colorado 80309, United States*

Complete contact information is available at: https://pubs.acs.org/10.1021/acs.est.1c00131

Notes

The authors declare no competing financial interest.

■ ACKNOWLEDGMENTS

This work was supported by the National Natural Science Foundation of China (41975158, 42011530176, and 41922037), the Shenzhen Science and Technology Innovation Committee (KCXFZ202002011008038), and the Guangdong Basic and Applied Basic Research Fund Committee (2020B1515130003). H.C. and D.H. acknowledge support from NASA (80NSSC18K0689 and NNX16AQ26G). Computational resources were provided by the Center for Computational Science and Engineering at the Southern University of Science and Technology.

■ REFERENCES

(1) Wang, T.; Xue, L.; Brimblecombe, P.; Lam, Y. F.; Li, L.; Zhang, L. Ozone Pollution in China: A Review of Concentrations, Meteorological Influences, Chemical Precursors, and Effects. *Sci. Total Environ.* **2017**, *575*, 1582−1596.

(2) Li, K.; Jacob, D. J.; Liao, H.; Shen, L.; Zhang, Q.; Bates, K. H. Anthropogenic Drivers of 2013−2017 Trends in Summer Surface Ozone in China. *Proc. Natl. Acad. Sci.* **2019**, *116*, 422−427.

(3) Lu, X.; Zhang, L.; Wang, X.; Gao, M.; Li, K.; Zhang, Y.; Yue, X.; Zhang, Y. Rapid Increases in Warm-Season Surface Ozone and Resulting Health Impact in China Since 2013. *Environ. Sci. Technol. Lett.* **2020**, *7*, 240−247.

(4) Ministry of Ecology and Environment of the People's Republic of China. *2019 Report on the State of the Ecology and Environment in China*; 2020. http://www.mee.gov.cn/hjzl/sthjzk/zghjzkgb/202006/P020200602509464172096.pdf.

(5) World Health Organization. *WHO Air Quality Guidelines for Particulate Matter, Ozone, Nitrogen Dioxide and Sulfur Dioxide: Global Update 2005: Summary of Risk Assessment*; 2006. https://apps.who.int/iris/bitstream/handle/10665/69477/WHO_SDE_PHE_OEH_06.02_eng.pdf;sequence=1.

(6) Ministry of Ecology and Environment of the People's Republic of China. *The Comprehensive Management Plan for Volatile Organic Compounds in Key Industries*; 2019. http://www.mee.gov.cn/xxgk2018/xxgk/xxgk03/201907/t20190703_708395.html.

(7) Liu, H.; Zhang, M.; Han, X. A Review of Surface Ozone Source Apportionment in China. *Atmos. Oceanic Sci. Lett.* **2020**, *13*, 470−484.

(8) Jun-Lin, A.; Yue-Si, W.; Fang-Kun, W.; Bin, Z. Characterizations of Volatile Organic Compounds during High Ozone Episodes in Beijing, China. *Environ. Monit. Assess.* **2012**, *184*, 1879−1889.

(9) Li, L.; Xie, S.; Zeng, L.; Wu, R.; Li, J. Characteristics of Volatile Organic Compounds and Their Role in Ground-Level Ozone Formation in the Beijing-Tianjin-Hebei Region, China. *Atmos. Environ.* **2015**, *113*, 247−254.

(10) Wu, R.; Xie, S. Spatial Distribution of Ozone Formation in China Derived from Emissions of Speciated Volatile Organic Compounds. *Environ. Sci. Technol.* **2017**, *51*, 2574−2583.

(11) Jiang, M.; Lu, K.; Su, R.; Tan, Z.; Wang, H.; Li, L.; Fu, Q.; Zhai, C.; Tan, Q.; Yue, D.; Chen, D.; Wang, Z.; Xie, S.; Zeng, L.; Zhang, Y. Ozone formation and key VOCs in typical Chinese city clusters. *Chin. Sci. Bull.* **2018**, *63*, 1130−1141.

(12) Liu, Y.; Song, M.; Liu, X.; Zhang, Y.; Hui, L.; Kong, L.; Zhang, Y.; Zhang, C.; Qu, Y.; An, J.; Ma, D.; Tan, Q.; Feng, M. Characterization and Sources of Volatile Organic Compounds (VOCs) and Their Related Changes during Ozone Pollution Days in 2016 in Beijing, China. *Environ. Pollut.* **2020**, *257*, 113599.

(13) Li, G.; Bei, N.; Cao, J.; Wu, J.; Long, X.; Feng, T.; Dai, W.; Liu, S.; Zhang, Q.; Tie, X. Widespread and Persistent Ozone Pollution in Eastern China during the Non-Winter Season of 2015: Observations and Source Attributions. *Atmos. Chem. Phys.* **2017**, *17*, 2759−2774.

(14) Gong, C.; Liao, H.; Zhang, L.; Yue, X.; Dang, R.; Yang, Y. Persistent Ozone Pollution Episodes in North China Exacerbated by Regional Transport. *Environ. Pollut.* **2020**, *265*, 115056.

(15) Liu, H.; Zhang, M.; Han, X.; Li, J.; Chen, L. Episode Analysis of Regional Contributions to Tropospheric Ozone in Beijing Using a Regional Air Quality Model. *Atmos. Environ.* **2019**, *199*, 299−312.

(16) Wang, P.; Chen, Y.; Hu, J.; Zhang, H.; Ying, Q. Source Apportionment of Summertime Ozone in China Using a Source-Oriented Chemical Transport Model. *Atmos. Environ.* **2019**, *211*, 79−90.

(17) Gao, M.; Gao, J.; Zhu, B.; Kumar, R.; Lu, X.; Song, S.; Zhang, Y.; Jia, B.; Wang, P.; Beig, G.; Hu, J.; Ying, Q.; Zhang, H.; Sherman, P.; McElroy, M. B. Ozone Pollution over China and India: Seasonality and Sources. *Atmos. Chem. Phys.* **2020**, *20*, 4399−4414.

(18) Gong, C.; Liao, H. A Typical Weather Pattern for Ozone Pollution Events in North China. *Atmos. Chem. Phys.* **2019**, *19*, 13725−13740.

(19) Han, H.; Liu, J.; Shu, L.; Wang, T.; Yuan, H. Local and Synoptic Meteorological Influences on Daily Variability in Summertime Surface Ozone in Eastern China. *Atmos. Chem. Phys.* **2020**, *20*, 203−222.

(20) Liu, Y.; Wang, T. Worsening Urban Ozone Pollution in China from 2013 to 2017 − Part 1: The Complex and Varying Roles of Meteorology. *Atmos. Chem. Phys.* **2020**, *20*, 6305−6321.

(21) Schmidt, H.; Martin, D. Adjoint Sensitivity of Episodic Ozone in the Paris Area to Emissions on the Continental Scale. *J. Geophys. Res.: Atmos.* **2003**, *108*, 8561.

(22) Hakami, A.; Seinfeld, J. H.; Chai, T.; Tang, Y.; Carmichael, G. R.; Sandu, A. Adjoint Sensitivity Analysis of Ozone Nonattainment over the Continental United States. *Environ. Sci. Technol.* **2006**, *40*, 3855−3864.

(23) Walker, T. W.; Jones, D. B. A.; Parrington, M.; Henze, D. K.; Murray, L. T.; Bottenheim, J. W.; Anlauf, K.; Worden, J. R.; Bowman, K. W.; Shim, C.; Singh, K.; Kopacz, M.; Tarasick, D. W.; Davies, J.; von der Gathen, P.; Thompson, A. M.; Carouge, C. C. Impacts of Midlatitude Precursor Emissions and Local Photochemistry on Ozone Abundances in the Arctic. *J. Geophys. Res.: Atmos.* **2012**, *117*, DOI: 10.1029/2011JD016370.

(24) Wang, M. Y.; Yim, S. H. L.; Wong, D. C.; Ho, K. F. Source Contributions of Surface Ozone in China Using an Adjoint Sensitivity Analysis. *Sci. Total Environ.* **2019**, *662*, 385−392.
(25) Zheng, B.; Tong, D.; Li, M.; Liu, F.; Hong, C.; Geng, G.; Li, H.; Li, X.; Peng, L.; Qi, J.; Yan, L.; Zhang, Y.; Zhao, H.; Zheng, Y.; He, K.; Zhang, Q. Trends in China's Anthropogenic Emissions since 2010 as the Consequence of Clean Air Actions. *Atmos. Chem. Phys.* **2018**, *18*, 14095−14111.
(26) Li, M.; Zhang, Q.; Zheng, B.; Tong, D.; Lei, Y.; Liu, F.; Hong, C.; Kang, S.; Yan, L.; Zhang, Y.; Bo, Y.; Su, H.; Cheng, Y.; He, K. Persistent Growth of Anthropogenic Non-Methane Volatile Organic Compound (NMVOC) Emissions in China during 1990−2017: Drivers, Speciation and Ozone Formation Potential. *Atmos. Chem. Phys.* **2019**, *19*, 8897−8913.
(27) Zhang, L.; Liu, L.; Zhao, Y.; Gong, S.; Zhang, X.; Henze, D. K.; Capps, S. L.; Fu, T.-M.; Zhang, Q.; Wang, Y. Source Attribution of Particulate Matter Pollution over North China with the Adjoint Method. *Environ. Res. Lett.* **2015**, *10*, No. 084011.
(28) An, X. Q.; Zhai, S. X.; Jin, M.; Gong, S.; Wang, Y. Development of an Adjoint Model of GRAPES−CUACE and Its Application in Tracking Influential Haze Source Areas in North China. *Geosci. Model Dev.* **2016**, *9*, 2153−2165.
(29) Pappin, A. J.; Hakami, A. Attainment vs Exposure: Ozone Metric Responses to Source-Specific NO_x Controls Using Adjoint Sensitivity Analysis. *Environ. Sci. Technol.* **2013**, *47*, 13519−13527.
(30) Lee, C. J.; Martin, R. V.; Henze, D. K.; Brauer, M.; Cohen, A.; Donkelaar, A. V. Response of Global Particulate-Matter-Related Mortality to Changes in Local Precursor Emissions. *Environ. Sci. Technol.* **2015**, *49*, 4335−4344.
(31) Lu, X.; Hong, J.; Zhang, L.; Cooper, O. R.; Schultz, M. G.; Xu, X.; Wang, T.; Gao, M.; Zhao, Y.; Zhang, Y. Severe Surface Ozone Pollution in China: A Global Perspective. *Environ. Sci. Technol. Lett.* **2018**, *5*, 487−494.
(32) Ministry of Environmental Protection of China (now Ministry of Ecology and Environment of the People's Republic of China). *Technical Regulation on Ambient Air Quality Index (on Trial)*; 2013. http://www.mee.gov.cn/ywgz/fgbz/bz/bzwb/jcffbz/201203/W020120410332725219541.pdf.
(33) Ministry of Environmental Protection of China (now Ministry of Ecology and Environment of the People's Republic of China). *Ambient Air Quality Standards*; 2012. http://www.mee.gov.cn/ywgz/fgbz/bz/bzwb/dqhjbh/dqhjzlbz/201203/W020120410330232398521.pdf.
(34) Ministry of Environmental Protection of China (now Ministry of Ecology and Environment of the People's Republic of China). *Amendment to the Ambient Air Quality Standards*; 2018. http://www.mee.gov.cn/xxgk2018/xxgk/xxgk01/201808/t20180815_629602.html.
(35) De Smedt, I.; Theys, N.; Yu, H.; Danckaert, T.; Lerot, C.; Compernolle, S.; Van Roozendael, M.; Richter, A.; Hilboll, A.; Peters, E.; Loyola, D.; Beirle, S.; Wagner, T.; Eskes, H.; Geffen, J. V.; Folkert Boersma, K.; Veefkind, P. Algorithm Theoretical Baseline for Formaldehyde Retrievals from S5P TROPOMI and from the QA4ECV Project. *Atmos. Meas. Tech.* **2018**, *11*, 2395.
(36) Van Geffen, J.; Boersma, K. F.; Eskes, H.; Sneep, M.; Ter Linden, M.; Zara, M.; Veefkind, J. P. S5P TROPOMI NO_2 Slant Column Retrieval: Method, Stability, Uncertainties and Comparisons with OMI. *Atmos. Meas. Tech.* **2020**, *13*, 1315−1335.
(37) Martin, R. V.; Fiore, A. M.; Van Donkelaar, A. Space-Based Diagnosis of Surface Ozone Sensitivity to Anthropogenic Emissions. *Geophys. Res. Lett.* **2004**, *31*, DOI: 10.1029/2004GL019416.
(38) Duncan, B. N.; Yoshida, Y.; Olson, J. R.; Sillman, S.; Martin, R. V.; Lamsal, L.; Hu, Y.; Pickering, K. E.; Retscher, C.; Allen, D. J.; Crawford, J. H. Application of OMI Observations to a Space-Based Indicator of NO_x and VOC Controls on Surface Ozone Formation. *Atmos. Environ.* **2010**, *44*, 2213−2223.
(39) Jin, X.; Fiore, A. M.; Murray, L. T.; Valin, L. C.; Lamsal, L. N.; Duncan, B.; Folkert Boersma, K.; De Smedt, I.; Abad, G. G.; Chance, K.; Tonnesen, G. S. Evaluating a Space-Based Indicator of Surface Ozone-NO_x-VOC Sensitivity Over Midlatitude Source Regions and Application to Decadal Trends. *J. Geophys. Res.: Atmos.* **2017**, *122*, 10,439−10,461.
(40) Veefkind, J. P.; Aben, I.; McMullan, K.; Förster, H.; de Vries, J.; Otter, G.; Claas, J.; Eskes, H. J.; de Haan, J. F.; Kleipool, Q.; van Weele, M.; Hasekamp, O.; Hoogeveen, R.; Landgraf, J.; Snel, R.; Tol, P.; Ingmann, P.; Voors, R.; Kruizinga, B.; Vink, R.; Visser, H.; Levelt, P. F. TROPOMI on the ESA Sentinel-5 Precursor: A GMES Mission for Global Observations of the Atmospheric Composition for Climate, Air Quality and Ozone Layer Applications. *Remote Sens. Environ.* **2012**, *120*, 70−83.
(41) Van Geffen, J. H. G. M.; Eskes, H. J.; Boersma, K. F.; Maasakkers, J. D.; Veefkind, J. P. TROPOMI ATBD of the Total and Tropospheric NO_2 Data Products. *DLR document* **2019** http://www.tropomi.eu/sites/default/files/files/publicSentinel-5P-TROPOMI-ATBD-NO2-data-products.pdf.
(42) Bey, I.; Jacob, D. J.; Yantosca, R. M.; Logan, J. A.; Field, B. D.; Fiore, A. M.; Li, Q.; Liu, H. Y.; Mickley, L. J.; Schultz, M. G. Global Modeling of Tropospheric Chemistry with Assimilated Meteorology: Model Description and Evaluation. *J. Geophys. Res.: Atmos.* **2001**, *106*, 23073−23095.
(43) Henze, D. K.; Hakami, A.; Seinfeld, J. H. Development of the Adjoint of GEOS-Chem. *Atmos. Chem. Phys.* **2007**, *7*, 2413−2433.
(44) Henze, D. K.; Seinfeld, J. H.; Shindell, D. T. Inverse Modeling and Mapping US Air Quality Influences of Inorganic $PM_{2.5}$ Precursor Emissions Using the Adjoint of GEOS-Chem. *Atmos. Chem. Phys.* **2009**, *9*, 5877−5903.
(45) Park, R. J.; Jacob, D. J.; Field, B. D.; Yantosca, R. M.; Chin, M. Natural and Transboundary Pollution Influences on Sulfate-Nitrate-Ammonium Aerosols in the United States: Implications for Policy. *J. Geophys. Res.: Atmos.* **2004**, *109*, D15204.
(46) Goliff, W. S.; Stockwell, W. R.; Lawson, C. V. The Regional Atmospheric Chemistry Mechanism, Version 2. *Atmos. Environ.* **2013**, *68*, 174−185.
(47) Li, M.; Zhang, Q.; Streets, D. G.; He, K. B.; Cheng, Y. F.; Emmons, L. K.; Huo, H.; Kang, S. C.; Lu, Z.; Shao, M.; Su, H.; Yu, X.; Zhang, Y. Mapping Asian Anthropogenic Emissions of Non-Methane Volatile Organic Compounds to Multiple Chemical Mechanisms. *Atmos. Chem. Phys.* **2014**, *14*, 5617−5638.
(48) Li, M.; Klimont, Z.; Zhang, Q.; Martin, R. V.; Zheng, B.; Heyes, C.; Cofala, J.; Zhang, Y.; He, K. Comparison and Evaluation of Anthropogenic Emissions of SO_2 and NO_x over China. *Atmos. Chem. Phys.* **2018**, *18*, 3433−3456.
(49) Elguindi, N.; Granier, C.; Stavrakou, T.; Darras, S.; Bauwens, M.; Cao, H.; Chen, C.; Denier van der Gon, H. A. C.; Dubovik, O.; Fu, T. M.; Henze, D. K.; Jiang, Z.; Keita, S.; Kuenen, J. J. P.; Kurokawa, J.; Liousse, C.; Miyazaki, K.; Müller, J.-F.; Qu, Z.; Solmon, F.; Zheng, B. Intercomparison of Magnitudes and Trends in Anthropogenic Surface Emissions From Bottom-Up Inventories, Top-Down Estimates, and Emission Scenarios. *Earth's Future* **2020**, *8*, No. e2020EF001520.
(50) Li, M.; Zhang, Q.; Kurokawa, J.; Woo, J.-H.; He, K.; Lu, Z.; Ohara, T.; Song, Y.; Streets, D. G.; Carmichael, G. R.; Cheng, Y.; Hong, C.; Huo, H.; Jiang, X.; Kang, S.; Liu, F.; Su, H.; Zheng, B. MIX: A Mosaic Asian Anthropogenic Emission Inventory under the International Collaboration Framework of the MICS-Asia and HTAP. *Atmos. Chem. Phys.* **2017**, *17*, 935−963.
(51) Price, C.; Rind, D. A Simple Lightning Parameterization for Calculating Global Lightning Distributions. *J. Geophys. Res.: Atmos.* **1992**, *97*, 9919−9933.
(52) Yienger, J. J.; Levy, H., II Empirical Model of Global Soil-Biogenic NO_x Emissions. *J. Geophys. Res.: Atmos.* **1995**, *100*, 11447.
(53) Guenther, A. B.; Jiang, X.; Heald, C. L.; Sakulyanontvittaya, T.; Duhl, T.; Emmons, L. K.; Wang, X. The Model of Emissions of Gases and Aerosols from Nature Version 2.1 (MEGAN2.1): An Extended and Updated Framework for Modeling Biogenic Emission. *Geosci. Model Dev.* **2012**, *5*, 1471−1492.
(54) van der Werf, G. R.; Randerson, J. T.; Giglio, L.; van Leeuwen, T. T.; Chen, Y.; Rogers, B. M.; Mu, M.; van Marle, M. J. E.; Morton,

https://doi.org/10.1021/acs.est.1c00131
Environ. Sci. Technol. XXXX, XXX, XXX−XXX

D. C.; Collatz, G. J.; Yokelson, R. J.; Kasibhatla, P. S. Global Fire Emissions Estimates during 1997−2016. *Earth Syst. Sci. Data* **2017**, *9*, 697−720.

(55) Young, P. J.; Naik, V.; Fiore, A. M.; Gaudel, A.; Guo, J.; Lin, M. Y.; Neu, J. L.; Parrish, D. D.; Rieder, H. E.; Schnell, J. L.; Tilmes, S.; Wild, O.; Zhang, L.; Ziemke, J.; Brandt, J.; Delcloo, A.; Doherty, R. M.; Geels, C.; Hegglin, M. I.; Hu, L.; Im, U.; Kumar, R.; Luhar, A.; Murray, L.; Plummer, D.; Rodriguez, J.; Saiz-Lopez, A.; Schultz, M. G.; Woodhouse, M. T.; Zeng, G. Tropospheric Ozone Assessment Report: Assessment of Global-Scale Model Performance for Global and Regional Ozone Distributions, Variability, and Trends. *Elementa: Sci. Anthropocene* **2018**, *6*, 10.

(56) Lu, X.; Zhang, L.; Chen, Y.; Zhou, M.; Zheng, B.; Li, K.; Liu, Y.; Lin, J.; Fu, T.-M.; Zhang, Q. Exploring 2016−2017 Surface Ozone Pollution over China: Source Contributions and Meteorological Influences. *Atmos. Chem. Phys.* **2019**, *19*, 8339−8361.

(57) Wang, W.; van der, A. R.; Ding, J.; van Weele, M.; Cheng, T. Spatial and temporal changes of the ozone sensitivity in China based on satellite and ground-based observations. *Atmos. Chem. Phys. Discuss.* **2020**, 1−24.

(58) Bari, M. A.; Kindzierski, W. B. Ambient Volatile Organic Compounds (VOCs) in Calgary, Alberta: Sources and Screening Health Risk Assessment. *Sci. Total Environ.* **2018**, *631-632*, 627−640.

(59) Jin, X.; Holloway, T. Spatial and Temporal Variability of Ozone Sensitivity over China Observed from the Ozone Monitoring Instrument. *J. Geophys. Res.: Atmos.* **2015**, *120*, 7229−7246.

(60) Lu, H.; Lyu, X.; Cheng, H.; Ling, Z.; Guo, H. Overview on the Spatial−Temporal Characteristics of the Ozone Formation Regime in China. *Environ. Sci.: Processes Impacts* **2019**, *21*, 916−929.

(61) Tang, G.; Liu, Y.; Zhang, J.; Liu, B.; Li, Q.; Sun, J.; Wang, Y.; Xuan, Y.; Li, Y.; Pan, J.; Li, X.; Wang, Y. Bypassing the NO_x Titration Trap in Ozone Pollution Control in Beijing. *Atmos. Res.* **2021**, *249*, 105333.

(62) Zhang, Q.; Zheng, Y.; Tong, D.; Shao, M.; Wang, S.; Zhang, Y.; Xu, X.; Wang, J.; He, H.; Liu, W.; Ding, Y.; Lei, Y.; Li, J.; Wang, Z.; Zhang, X.; Wang, Y.; Cheng, J.; Liu, Y.; Shi, Q.; Yan, L.; Geng, G.; Hong, C.; Li, M.; Liu, F.; Zheng, B.; Cao, J.; Ding, A.; Gao, J.; Fu, Q.; Huo, J.; Liu, B.; Liu, Z.; Yang, F.; He, K.; Hao, J. Drivers of improved $PM_{2.5}$ air quality in China from 2013 to 2017. *Proc. Natl. Acad. Sci.* **2019**, *116*, 24463−24469.

(63) Tang, G.; Zhu, X.; Xin, J.; Hu, B.; Song, T.; Sun, Y.; Zhang, J.; Wang, L.; Cheng, M.; Chao, N.; Kong, L.; Li, X.; Wang, Y. Modelling Study of Boundary-Layer Ozone over Northern China - Part I: Ozone Budget in Summer. *Atmos. Res.* **2017**, *187*, 128−137.

https://doi.org/10.1021/acs.est.1c00131
Environ. Sci. Technol. XXXX, XXX, XXX−XXX